AUTOCALIBRATED REGULARIZED PARALLEL MRI RECONSTRUCTION IN THE WAVELET DOMAIN

L. Chaari[1,3]*, J.- C. Pesquet*[1]*, A. Benazza-Benyahia*[2,1] *and Ph. Ciuciu*[3]

[1] IGM and UMR-CNRS 8049, Université Paris-Est
Champs-sur-Marne, 77454 Marne-la-Vallée, France
{chaari,pesquet}@univ-mlv.fr
[2] URISA, SUP'COM, Cité Technologique des Communications, 2083, Tunisia
benazza.amel@supcom.rnu.tn
[3] CEA/DSV/I^{2}BM/Neurospin
CEA Saclay, Bat. 145, Point Courrier 156, 91191 Gif-sur-Yvette cedex, France
philippe.ciuciu@cea.fr

ABSTRACT

To reduce the scanning time in some MRI applications, parallel acquisition techniques with multiple coils have been developed. Then, the full Field of View (FOV) image is reconstructed from the resulting registred subsampled k-space data. To this end, several reconstruction techniques have been proposed such as the widely-used SENSE method. However, the reconstructed image generally presents artifacts especially when perturbations occur in both the measured data and in the estimated coil sensitivity maps. In order to alleviate such shortcomings by limiting the distortions, Tikhonov regularization in the image domain has also been investigated. In this paper, we present a novel algorithm for SENSE reconstruction which proceeds with regularization in the wavelet domain, the hyperparameters being estimated from the data. Experiments carried out on real T1-weighted MRI data at 1.5 T indicate that the proposed algorithm generates reconstructed images with reduced artifacts in comparison with conventional reconstruction techniques.

Index Terms— SENSE, pMRI, reconstruction, wavelets, regularization, Bayesian approaches, convex optimization.

1. INTRODUCTION

Speeding up the MRI data acquisition is of main interest for studying the brain dynamics in (almost) real-time. To this purpose, parallel imaging has been developed: multiple receiver surface coils located around the underlying object are employed to simultaneously collect in the frequency domain (i.e the k-space) data sampled at a rate R times lower than the Nyquist sampling rate. Therefore, the total acquisition time is R times shorter than with conventional non parallel imaging. Then, a reconstruction step is performed to build a full FOV image from the subsampled ones by suppressing aliasing distortions. Several reconstruction methods like SMASH (Simultaneous acquisition of spatial harmonics) [1] and SENSE (Sensitivity Encoding) [2] have been developed in order to unfold the aliased registred images in the k-space and in the image domain, respectively. For instance, the widely-used SENSE technique amounts to a weighted least squares estimation in the image domain. Ideally, this method is supposed to achieve an exact reconstruction in the absence of noise. However, in practice, noisy data and inaccuracies in the coil sensitivity maps make the reconstruction task an ill-conditioned problem. Some alternatives have been proposed. The coil geometry can be optimized [3] and an improved estimation of coil sensitivity profiles can also be performed [4]. However, much attention was paid to regularization techniques in the reconstruction process [5, 6]. Most of them operate in the image domain.

Using a 1.5 T magnetic field, high reduction factors like $R = 4$ are considered as unfeasible since the reconstructed images are affected by severe aliasing artifacts. The objective of this work is to develop a regularized reconstruction technique in the wavelet domain that reduces these artifacts for high reduction factors and low magnetic field intensity. We will further show that this choice has been motivated by a tractable statistical modelling and a fast optimization procedure.

This paper is organized as follows. In Section 2, we give a brief overview of the SENSE method and its regularized version in the data domain. Section 3 is devoted to a detailed description of the proposed wavelet-based regularization procedure. Our approach is illustrated on T1-weighted anatomical data and results are commented in Section 4. Finally, some conclusions and perspectives concerning functional MRI data are drawn in Section 5.

2. BACKGROUND

2.1. Basic SENSE reconstruction

An array of L coils is employed to measure the spin density ρ into the object under investigation. The signal d_l received by each coil l ($1 \leq l \leq L$) is the Fourier transform of the desired image function ρ weighted by the coil sensitivity profile s_l evaluated at some $\vec{k}$ locations in the k-space which are defined by the sampling scheme:

$$d_l(\vec{k}) = \int \rho(\vec{r}) s_l(\vec{r}) e^{-\imath 2\pi \vec{k}^{\mathsf{T}} \vec{r}} d\vec{r}. \quad (1)$$

For the sake of simplicity, the Cartesian sampling is retained. Due to the separability of the Fourier transform, the problem amounts to a one-dimensional inversion along the phase encoding axis. Let $\Delta x = \frac{R}{X}$ be the sampling period with X the size of the FOV along the phase encoding direction, let x be the position in the image domain and $R \leq L$ the reduction factor. By accounting for the under-

This work was supported by grants from Région Ile de France.

sampling of the k-space by R, Eq. (1) admits the following matrix form:

$$\vec{d}(x) = \mathbf{S}(x)\vec{\rho}(x) \tag{2}$$

where

$$\mathbf{S}(x) \triangleq \begin{pmatrix} s_1(x) & \dots & s_1(x+(R-1)\Delta x) \\ \vdots & \vdots & \vdots \\ s_L(x) & \dots & s_L(x+(R-1)\Delta x) \end{pmatrix},$$

$$\vec{\rho}(x) \triangleq \begin{pmatrix} \rho(x) \\ \rho(x+\Delta x) \\ \vdots \\ \rho(x+(R-1)\Delta x) \end{pmatrix} \text{and} \quad \vec{d}(x) \triangleq \begin{pmatrix} d_1(x) \\ d_2(x) \\ \vdots \\ d_L(x) \end{pmatrix}.$$

As a consequence, the reconstruction step consists of recovering $\vec{\rho}(x)$ from $\vec{d}(x)$ at each voxel position indexed by x. Note that the data fields $(d_l)_{1\leq l\leq L}$ and the unknown image ρ are complex-valued, although $|\rho|$ is only considered for visualization purposes.

A simple reconstruction method is the SENSE approach, based on the conventional least squares estimator [2]. The objective is to find the vector $\widehat{\vec{\rho}}_{\mathrm{LS}}(x)$ that minimizes the residual least squares criterion weighted by the inverse of the between-coil noise covariance matrix $\mathbf{\Psi}$ of size $L \times L$:

$$\begin{aligned} \widehat{\vec{\rho}}_{\mathrm{LS}}(x) &= \arg\min_{\vec{\rho}(x)} \| \vec{d}(x) - \mathbf{S}(x)\vec{\rho}(x) \|^2_{\mathbf{\Psi}^{-1}} \\ &= \big(\mathbf{S}^{\mathsf{H}}(x)\mathbf{\Psi}^{-1}\mathbf{S}(x)\big)^{-1}\mathbf{S}^{\mathsf{H}}(x)\vec{d}(x), \end{aligned} \tag{3}$$

where $(\cdot)^{\mathsf{H}}$ stands for the transposed complex conjugate. In practice, several limitations drastically limit the performance of the SENSE method because of the presence of distortions in the measurements $\vec{d}(x)$ and in the estimation of $\mathbf{S}(x)$. These undesirable effects are illustrated in Fig. 1 which shows aliasing artifacts in the reconstructed images for two reduction factors: $R = 2$ and $R = 4$. To address this ill-conditioned problem, regularization is usually applied.

2.2. Tikhonov regularization

The Tikhonov regularization framework is usually considered by determining $\widehat{\vec{\rho}}_{\mathrm{reg}}(x)$ as the minimizer of the penalized criterion:

$$\mathcal{J}_{\mathrm{reg}}(\vec{\rho}(x)) = \| \vec{d}(x) - \mathbf{S}(x)\vec{\rho}(x) \|^2_{\mathbf{\Psi}^{-1}} + \mu \, \| \vec{\rho}(x) - \vec{\rho}_r(x) \|^2 \, . \tag{4}$$

The regularization parameter $\mu > 0$ ensures a balance between the closeness to the data and the penalty term which controls the deviation with respect to a reference vector $\vec{\rho}_r(x)$. The solution $\widehat{\vec{\rho}}_{\mathrm{reg}}(x)$ admits the following closed-form expression:

$$\begin{aligned} \widehat{\vec{\rho}}_{\mathrm{reg}}(x) = \quad & \vec{\rho}_r(x) + \big(\mathbf{S}^{\mathsf{H}}(x)\mathbf{\Psi}^{-1}\mathbf{S}(x) + \mu\mathbf{I}_R\big)^{-1}\mathbf{S}^{\mathsf{H}}(x)\mathbf{\Psi}^{-1} \\ & \times\big(\vec{d}(x) - \mathbf{S}(x)\vec{\rho}_r(x)\big), \end{aligned} \tag{5}$$

where $\mathbf{I}_R$ is the R-dimensional identity matrix. It is worth noticing that any quadratic regularization procedure introduces blurring effects except for specific values of μ (see Fig. 4 (left)). To overcome this limitation, one usually resorts to edge-preserving penalty terms. Here, we propose to apply edge-preserving penalty in the Wavelet Transform (WT) domain [7].

3. REGULARIZATION IN THE WT DOMAIN

3.1. Motivation

When carefully analyzing SENSE-based reconstructed images (see Fig. 1 for $R = 4$), artifacts appear as distorted curves with either very high or very low intensity, well spatially-localized. Consequently, we propose to look for an image representation where these localized transitions can be easily detected and hence attenuated. In this respect, the WT has been recognized as a powerful tool that enables a good space and frequency localization. In addition, as we will show, the statistics of the wavelet coefficients can also be easily modelled allowing us to efficiently employ a Bayesian framework for the estimation procedure.

3.2. Optimization criterion

In what follows, $\mathbf{T}$ stands for the WT operator. It corresponds to a discrete decomposition onto a separable 2D orthonormal wavelet basis performed over $j_{\max}$ resolution levels. In this context, we define the resulting wavelet coefficient field of the target image ρ by $\zeta = \big((\zeta_{a,m})_m, (\zeta_{h,j,m}, \zeta_{v,j,m}, \zeta_{d,j,m})_{1\leq j\leq j_{\max},m}\big)$ where $\zeta_{a,m}$ denotes an approximation coefficient at resolution level $j_{\max}$ and location m and $\zeta_{o,j,m}$ with $o \in \{h, v, d\}$ denotes a detail coefficient at resolution level j, location m and orientation o, which may be horizontal (h), vertical (v) or diagonal (d). We aim at building an estimate $\widehat{\zeta}$ of ζ from $\vec{d}$. Then, an estimate of the objective image is easily derived by just applying the inverse WT operator $\mathbf{T}^*$ to $\widehat{\zeta}$. For the sake of mathematical convenience, the maximum *a posteriori* (MAP) estimator is retained as solution:

$$\widehat{\zeta} = \arg\max_{\zeta} \big[\ln g(\vec{d} \mid \mathbf{T}^*\zeta) + \ln f(\zeta) \big], \tag{6}$$

where $g(\vec{d} \mid \mathbf{T}^*\zeta)$ is the likelihood of the observed data and $f(\zeta)$ is the prior probability density function of the image in the wavelet domain. Assuming an i.i.d Gaussian vector noise in the imaging process, the likelihood can be expressed as:

$$g(\vec{d} \mid \rho) \propto \exp\left(-G(\rho)\right) \tag{7}$$

where $G(\rho) = \frac{1}{2}\sum_x \| \vec{d}(x) - \mathbf{S}(x)\vec{\rho}(x) \|^2_{\mathbf{\Psi}^{-1}}$.

By analyzing the empirical distribution of the real and imaginary parts of the considered detail coefficients, it is observed that their histograms are well-fitted by generalized Gaussian distributions. The corresponding probability density function $f_{p,\alpha}$ depends on a shape exponent $p \in [1, \infty[$ and a scale parameter $\alpha \in \mathbb{R}_+^*$:

$$\forall \xi \in \mathbb{R}, \qquad f_{p,\alpha}(\xi) = \frac{p}{2\alpha^{1/p}\Gamma(\frac{1}{p})} e^{-\frac{|\xi|^p}{\alpha}}. \tag{8}$$

At the coarsest resolution level, the distributions of both the real and imaginary parts of the approximation coefficients can be modelled by a Gaussian distribution with mean μ and variance σ^2. Furthermore, we have found very low values of the correlation factors between the real and imaginary parts of the wavelet coefficients. This allows us to assume that the real and imaginary parts of wavelet coefficients are independent. For the sake of simplicity, we also assume that the real (resp. imaginary) parts of the wavelet coefficients form an independent sequence and they are identically distributed in each subband. So the MAP estimator is obtained as the minimizer of $\mathcal{J} = \mathcal{J}_1 + \mathcal{J}_2$ where $\mathcal{J}_1(\zeta) = G(\mathbf{T}^*\zeta)$ and

$$\mathcal{J}_2(\zeta) \;=\; \sum_m \Phi_a(\zeta_{a,m}) \;+\; \sum_{j=1}^{j_{\max}} \sum_{o\in\{h,v,d\}} \sum_m \Phi_{o,j}(\zeta_{o,j,m})$$

where

$$\Phi_a(\zeta_{a,m}) = \frac{(\mathrm{Re}(\zeta_{a,m}) - \mu^{\mathrm{Re}})^2}{2\sigma^2_{\mathrm{Re}}} + \frac{(\mathrm{Im}(\zeta_{a,m}) - \mu^{\mathrm{Im}})^2}{2\sigma^2_{\mathrm{Im}}}$$

$$\Phi_{o,j}(\zeta_{o,j,m}) = \frac{|\mathrm{Re}(\zeta_{o,j,m})|^{p^{\mathrm{Re}}_{j,o}}}{\alpha^{\mathrm{Re}}_{j,o}} + \frac{|\mathrm{Im}(\zeta_{o,j,m})|^{p^{\mathrm{Im}}_{j,o}}}{\alpha^{\mathrm{Im}}_{j,o}}$$

with $(p^{\mathrm{Re}}_{j,o}, p^{\mathrm{Im}}_{j,o}) \in [1,\infty[^2$ and $(\alpha^{\mathrm{Re}}_{j,o}, \alpha^{\mathrm{Re}}_{j,o}) \in (\mathbb{R}^*_+)^2$. Hereabove, $\mathrm{Re}(\cdot)$ and $\mathrm{Im}(\cdot)$ (or $\cdot^{\mathrm{Re}}$ and $\cdot^{\mathrm{Im}}$) respectively stand for the real and imaginary parts. In this context, the optimization procedure cannot rely on conventional convex optimization algorithms: although $\mathcal{J}_1$ is differentiable with a Lipschitz-continuous gradient, $\mathcal{J}_2$ is not even guaranteed to be differentiable. Therefore, we propose to apply the iterative optimization procedure developed in [8], which is a generalization of the previous work in [9].

3.3. Optimization algorithm

The goal of our algorithm is to iteratively compute a field of coefficients $\widehat{\zeta}$ that minimizes $\mathcal{J}$. For doing so, we will use the concept of *proximity operator* which was found to be fundamental in a number of recent works in convex optimization [10, 8] . In particular, the proximity operator of the function $\phi : \mathbb{R} \to \mathbb{R}, \xi \mapsto |\xi|^p/\alpha$ with $p \in [1,\infty[$ and $\alpha \in \mathbb{R}^*_+$ is:

- if $p = 1$, the soft thresholding operator defined by $\mathrm{prox}_\phi(\xi) = \mathrm{sign}(\xi)\max\{|\xi| - \alpha^{-1}, 0\}$;
- if $p \neq 1$, $\mathrm{prox}_\phi(\xi) = \mathrm{sign}(\xi)\eta$ where η is the unique solution in $[0,+\infty[$ to $\eta + p\eta^{p-1}/\alpha = |\xi|$.

We extend the definition of proximity operation to functions defined on conplex-valued objects. For $\Phi : \mathbb{C} \to \mathbb{R}, \xi \mapsto \phi^{\mathrm{Re}}(\mathrm{Re}(\xi)) + \phi^{\mathrm{Im}}(\mathrm{Im}(\xi))$, where ϕ^{Re} and ϕ^{Im} are convex functions of the same form as ϕ above, the proximity operator is defined as $\mathrm{prox}_\Phi(\xi) = \mathrm{prox}_{\phi^{\mathrm{Re}}}(\mathrm{Re}(\xi)) + \imath\mathrm{prox}_{\phi^{\mathrm{Im}}}(\mathrm{Im}(\xi))$. The functions $\Phi_{o,j}$ and Φ_a defined in the previous section are typically of the form of interest.

By extension to the complex case of the algorithm in [8], a minimizer of $\mathcal{J}$ can then be computed iteratively by setting, for every iteration $n \in \mathbb{N}$:

$$\zeta^{(n+1)}_{o,j,m} = \zeta^{(n)}_{o,j,m} + \lambda_n\Big(\mathrm{prox}_{\gamma_n\Phi_{o,j}}(\zeta^{(n)}_{o,j,m} - \gamma_n[\nabla\mathcal{J}_1(\zeta^{(n)})]_{o,j,m}) - \zeta^{(n)}_{o,j,m}\Big) \quad (9)$$

(a similar equation is used to update $\zeta^{(n)}_{a,m}$), where a closed-form expression of $[\nabla\mathcal{J}_1]_{o,j,m} = \frac{\partial\mathcal{J}_1}{\partial\mathrm{Re}(\zeta_{o,j,m})} + \imath\frac{\partial\mathcal{J}_1}{\partial\mathrm{Im}(\zeta_{o,j,m})}$ can easily be computed where $\lambda_n \in]0,1]$ and $\gamma_n \in]0, \gamma_{\max}[$ are respectively relaxation and step-size parameters ($2/\gamma_{\max}$ is the Lipschitz constant of $\nabla\mathcal{J}_1$). Results obtained with this iterative method are provided and discussed in the next section.

4. RESULTS

Experiments have been conducted on real data sets containing $256 \times 256 \times 14$ T1-weighted anatomical images with $0.93 \times 0.93 \times 8$ (mm) spatial resolution and a reduction factor $R = 4$. These images have been acquired with Signa 1.5 Tesla GE Healthcare scanner using an eight-channel head coil ($L = 8$). The illustrated reconstructed images correspond to the 14^{th} slice which is the most distorted one. We have used the Symlet 8 wavelet basis over 1, 2 or 3 resolution levels. The maximum likelihood estimator has been used to estimate all the hyper-parameters for the distributions of the real and imaginary parts of the approximation/detail coefficients. Fig. 2 illustrates the evolution of the optimization criterion with respect to the iteration number n when $j_{\max} = 1$, 2 and 3. It can be considered that, after about 80 iterations, the minimum has been reached. We are guaranteed that it corresponds to the optimal MAP solution. Using a reference image ρ_{ref} calculated with $R = 2$ and the reconstructed image ρ_{rec}, Fig. 3 provides the Signal to Noise Ratio (SNR=$20\log_{10}\frac{||\rho_{ref}||_2}{||\rho_{ref}-\rho_{rec}||_2}$) variation with respect to the iteration number for the same range of resolution levels. We note that the SNR increases with the number of resolution levels. Fig. 4 allows us to evaluate the difference between the image reconstruction using Tikhonov regularization (left) ($\mathrm{SNR} = 14$ dB) and the proposed WT algorithm (right) ($\mathrm{SNR} = 14.5$ dB). The comparison with the basic-SENSE reconstructed image can be made by referring to Fig. 1 (right) ($\mathrm{SNR} = 13.9$ dB). Note that blurring effects in the Tikhonov regularized image are no longer present in the WT regularized image. Moreover, the aliasing artifacts in the basic-SENSE reconstructed image are significantly smoothed with the proposed wavelet-based approach but they are completely removed only if they were not actually very strong. Fig. 5 displays the difference images between the reconstructed images at different resolution levels. It is clear that, by increasing the number of resolution levels, our algorithm converges faster while getting an improved reconstruction quality. However, slight improvements only are noticeable beyond 3 resolution levels.

5. CONCLUSION

We have proposed a novel Bayesian approach for SENSE reconstruction based on a regularization in a 2D orthonormal wavelet basis. This method reduces aliasing artifacts related to the noise in the acquired data, which become critical when using high reduction factors with low magnetic field intensity. Results show improvements in the reconstructed images compared with basic SENSE and some other regularization methods. The considered method can be adapted to functional MRI data, possibly taken into account time dependencies.

6. REFERENCES

[1] D. K. Sodickson and W. J. Manning, " Simultaneous acquisition of spatial harmonics (SMASH): fast imaging with radiofrequency coil arrays," *Magnetic Resonance in Medicine*, vol. 38, pp. 591-603, June 1999.

[2] K. P. Pruessmann, M. Weiger, M. B. Scheidegger and P. Boesiger, " SENSE : sensitivity encoding for fast MRI," *Magnetic Resonance in Medicine*, vol. 42, pp. 952-962, July 1999.

[3] M. Weiger, K. P. Pruessmann, C. Lessler, P. Roschmann and P. Boeisiger, " Specific coil design for sense: a six-element cardiac array," *Magnetic Resonance in Medicine*, vol. 45, pp. 495-504, 2001.

[4] M. Blaimer, F. Breuer, M. Mueller, R. M. Heidemann, M. A. Griswold, and P. M. Jakob, " SMASH, SENSE, PILS, GRAPPA: How to choose the optimal method," *Magnetic Resonance in Medicine*, vol. 15, pp. 223-236, August 2004.

[5] L. Ying, D. Xu and Z.-P. Liang, " On Tikhonov regularization for image reconstruction in parallel MRI," *IEEE Engineering in Medicine and Biology Society*, vol. 2, pp. 1056-1059, September 2004.

[6] C. Rabrait, Ph. Ciuciu, A. Ribès, C. Poupon, P. Leroux, V. Lebon, G. Dehaene-Lambertz, D. Le Bihan and F. Lethimonnier, " High temporal resolution functional MRI using parallel echo volume imaging," *Journal of Magnetic Resonance Imaging*, In Press, April 2008.

[7] S. Mallat, " A wavelet tour of signal processing," *Academic Press*, 1998.

[8] C. Chaux, P. Combettes, J.-C. Pesquet and V. R. Wajs, " A variational formulation for frame-based inverse problems," *Inverse Problems*, vol. 23, pp. 1495-1518, August 2007.

[9] I. Daubechies, M. Defrise and C. DeMol, " An iterative thresholding algorithm for linear inverse problems with a sparsity constraint," *Comm. Pure Appl. Math.*, vol. 57, pp. 1413-1457, 2004.

[10] P. L. Combettes and V. R. Wajs, " Signal recovery by proximal forward-backward splitting," *Multiscale Model. Simul.*, vol. 4, pp. 1168-1200, 2005.

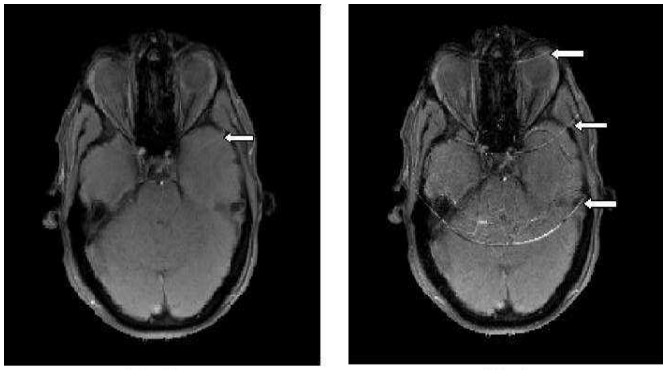

Fig. 1. White arrows indicate the aliasing artifacts in the reconstructed image using the basic SENSE algorithm with $R = 2$ (left) and $R = 4$ (right).

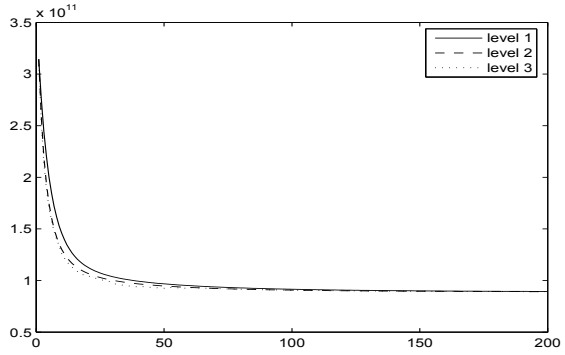

Fig. 2. Variation of the optimization criterion $\mathcal{J}$ w.r.t. iteration number n for $j_{\max} \in \{1, 2, 3\}$ ($\lambda_n = 0.1$ and $\gamma_n = 0.7$).

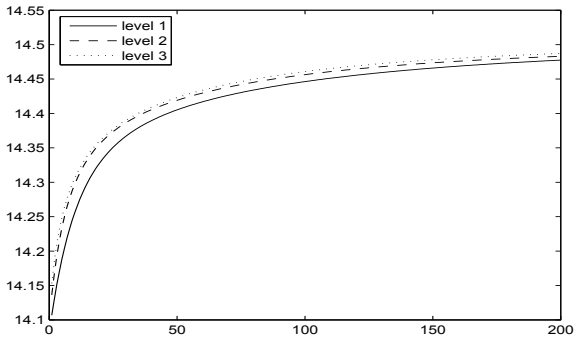

Fig. 3. Variation of SNR in dB w.r.t. iteration number n for $j_{\max} \in \{1, 2, 3\}$ ($\lambda_n = 0.1$ and $\gamma_n = 0.7$).

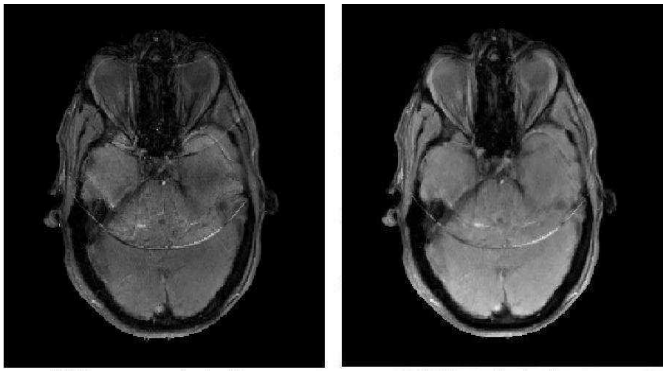

Fig. 4. Reconstructed image using Tikhonov regularization (left) and WT regularization (right) with $R = 4$.

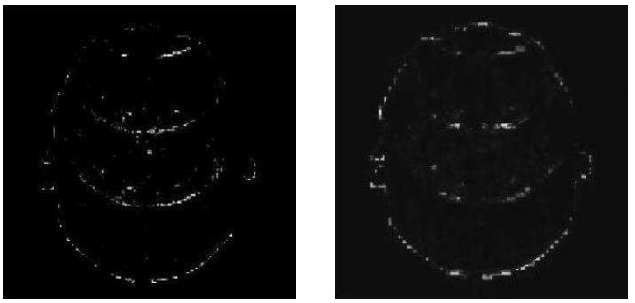

(Image with $j_{\max} = 1$)−(Image with $j_{\max} = 2$) (Image with $j_{\max} = 2$)−(Image with $j_{\max} = 3$)

Fig. 5. Difference between images reconstructed at different resolution levels